Minimization of the DC Current Ripple of a Three-Phase Buck+Boost PWM Unity Power Factor Rectifier

Martina Baumann
Vienna University of Technology
Department of Electrical Drives and Machines
Gusshausstrasse 27/E372
A – 1040 Vienna/Austria
phone: +43-1-58801 37225, fax: +43-1-58801 37298
email: martina.baumann@tuwien.ac.at

Johann W. Kolar
Swiss Federal Institute of Technology (ETH) Zurich
Power Electronic Systems Laboratory
ETH-Zentrum / ETL H22
CH – 8092 Zurich/Switzerland
phone: +41-1-632 2834, fax: +41-1-632 1212
email: kolar@lem.ee.ethz.ch

Abstract – *The modulation of a novel three-phase three-switch buck-type unity power factor rectifier with integrated DC/DC boost converter output stage is optimized concerning the ripple amplitude of the buck+boost inductor current. This is achieved by coordination of the switching operation of the buck input stage and of the boost output stage. A comparative evaluation of different modulation schemes does identify a modulation scheme which simultaneously does provide minimum DC current ripple and minimum input filter capacitor voltage ripple at minimum switching losses and/or maximum pulse frequency. All theoretical considerations are for operation in a wide input voltage range and are verified by simulations and by measurements on a DSP-controlled 5kW prototype of the system.*

Key words: three-phase PWM rectifier, buck type converter, buck+boost inductor, inductor current ripple minimization.

1 Introduction

In [1] a novel three-phase three-switch buck-type unity power factor PWM rectifier with integrated DC/DC boost converter output stage (three-phase buck+boost PWM rectifier) has been presented (cf. **Fig. 1**), which does allow to control the output voltage to a constant value of $U_0 = 400\,\mathrm{V}$ within an universal input voltage range of $U_{N,l-l} = (208 \ldots 480)\,\mathrm{V_{rms}}$ line-to-line [2].

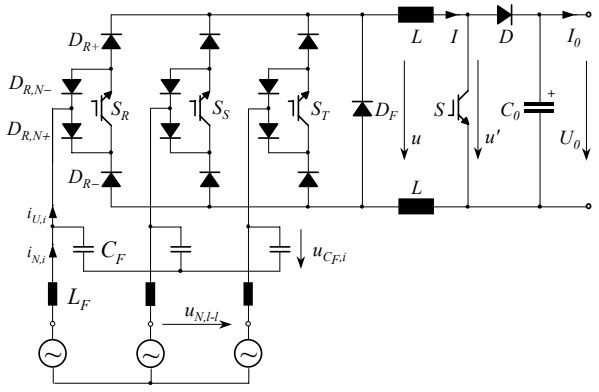

Fig. 1: Structure of the power circuit of the three-phase buck+boost PWM rectifier.

The three-phase buck+boost PWM rectifier shows the following main advantages:

- sinusoidal shape of the input currents
- resistive fundamental mains behavior
- possibility of limiting the input current and/or the current in the buck+boost inductor for mains overvoltages
- high efficiency (up to $\eta = 97\%$)
- high power density ($\rho = 965\,\mathrm{W/dm^3}$ or $15.8\,\mathrm{W/in^3}$).

Furthermore, in contrast to rectifier systems with boost-type input stage

- no auxiliary start-up circuit

is required.

An experimental setup of the three-phase buck+boost PWM rectifier has been realized using standard power semiconductors (in TO 247 packages) and a digital signal processor ADSP-21061 SHARC (Analog Devices) for the implementation of the system control. The specifications of the system prototype are:

$$\begin{array}{llll} P_0 & = 5\,\mathrm{kW} & f_N & = 50\,\mathrm{Hz} \\ U_{N,l-l} & = 208\,\mathrm{V} \ldots 480\,\mathrm{V} & f_P & = 23.4\,\mathrm{kHz} \\ U_0 & = 400\,\mathrm{V} & & \end{array}$$

(f_N denotes the mains frequency, f_P denotes the pulse frequency). There are different modulation methods available, which differ concerning

- switching losses,
- input filter capacitor voltage ripple,
- time behavior of the buck+boost inductor current ripple,

and concerning the minimum load at which the

- transition between continuous buck+boost inductor current (CCM) and discontinuous buck+boost inductor current (DCM) does occur.

In [4] an optimization of the modulation scheme concerning the AC side system behavior has been proposed which does provide a minimum rms value of the input filter capacitor voltage ripple and minimum switching losses. However, as a comparison of the size and/or of the weight of the input filter capacitors and of the buck+boost inductor shows, an optimization concerning the DC side could be more useful as compared to an AC side optimization in order to reduce the size and the weight of the heavy buck+boost inductor and to increase the specific power (W/kg). Currently, the size of the buck+boost inductor is $327\,\mathrm{cm}^3$[1], the input filter capacitors are approximately 40 % smaller in size. The difference in weight is even more significant: the weight of the buck+boost inductors is 1500 g, the weight of the input filter capacitors is only 300 g. The implemented components are depicted in **Fig. 2**(a), Fig. 2(b) shows the relations between size and weight.

In this paper the modulation of the three-phase buck+boost PWM rectifier for operation in a wide input voltage range is optimized concerning the buck+boost inductor current ripple, and all theoretical considerations are verified by simulations and by measurements on the DSP-controlled 5 kW prototype of the system. It is interesting to note, that to the knowledge of the authors the ripple of the DC output current of a high frequency three-phase buck type PWM converter has not been considered in the optimization of modulation schemes in the literature so far. (Also for boost-type systems only a very limited number of papers is available on the analysis of the ripple of the DC side quantity, cf. e.g. [3].) In **section 2** of the paper the basic principle of operation of the three-phase buck+boost PWM rectifier is described briefly. **Section 3** treats the different

[1] Dimensions: diameter ≈ 6cm(2.4in), height ≈ 6cm(2.4in)

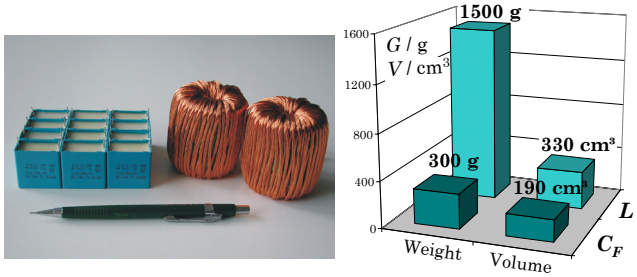

(a) (b)

Fig. 2: Comparison of weight and volume of the input filter capacitors C_F and of the buck+boost inductors L employed in the prototype of the 5kW three-phase wide input voltage range buck+boost PWM rectifier: **(a)** Physical appearance and **(b)** volume and weight.

modulation methods which are available for the control of the buck and of the boost stage. Based on this, the ripple of the buck+boost inductor current is analyzed in **section 4**. There, the time behavior of the ripple current and its envelope are calculated analytically for the different modulation methods. Furthermore, the rms value of the current ripple is calculated in analytically closed form in order to provide a basis for the estimation of the copper losses of the buck+boost inductor. Finally, the theoretical considerations are verified by simulations (cf. **section 5**) and by experimental investigations in **section 6**.

2 Principle of Operation

In the following, the basic principle of operation of the system shown in Fig. 1 is discussed briefly. Based on the investigation of the conduction states several possibilities for arranging the switching states within one pulse period, resulting in different modulation methods are analyzed.

Due to the phase symmetry of the converter structure and based on the assumed symmetry of the mains voltage system, the investigation can be limited to a $\frac{\pi}{6}$-wide interval of the mains period. In the case at hand we will consider a combination of the mains phase voltages

$$u_{N,R} > 0 > u_{N,S} > u_{N,T} \tag{1}$$

being valid within the mains angle interval $\varphi_U \in (0; \frac{\pi}{6})$, in case the mains voltage $u_{N,i}$ is defined as

$$\begin{aligned} u_{N,R} &= \hat{U}_N \cos(\omega_N t), \\ u_{N,S} &= \hat{U}_N \cos(\omega_N t - 2\pi/3), \\ u_{N,T} &= \hat{U}_N \cos(\omega_N t + 2\pi/3). \end{aligned} \tag{2}$$

For the characterization of a switching state of the system we use the combination $j = (s_R s_S s_T)$ of the phase switching functions s_i. There, the switching function does define the switching state of the corresponding power transistor, where $s_i = 0$ denotes the off-state, and $s_i = 1$ denotes the on-state. In **Fig. 3** the conduction states of the buck stage are given for the considered mains interval (cf. (1)).

For achieving a resistive fundamental mains behavior, $i_{N,i} \sim u_{N,i}$, and for neglecting the fundamental of the input filter capacitor currents ($i_{N,i} \approx i_{U,(1),i}$) fundamentals

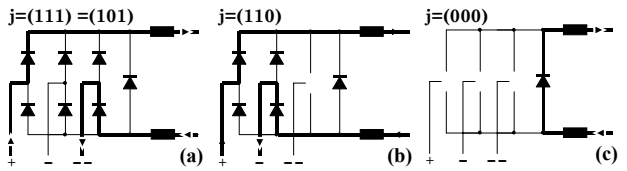

Fig. 3: Conduction states of the buck stage (valid for filter capacitor phase voltage relation according to (1)). The current flow is indicated by a bold line, and the power transistors are not explicitly shown for the sake of clearness. **(a)** and **(b):** active switching states, **(c)**: free-wheeling state.

$i_{U,(1),i}$ of the discontinuous rectifier input phase currents $i_{U,i}$ lying in phase with the corresponding mains phase voltage $u_{N,i}$ ($\approx u_{C_F,i}$) have to be formed. Accordingly, the relative on-times of the power transistors S_i of the buck input stage have to be set proportional to the instantaneous value of the mains phase voltages. There, the buck stage output current I is assumed to be approximately constant and impressed by the buck+boost inductor. With the modulation index M of the buck input stage

$$M = \frac{\hat{I}_N}{I} = \frac{\sqrt{2}\,U}{\sqrt{3}\,U_{N,l-l}} \qquad M \in [0;1], \tag{3}$$

(where $\hat{I}_N$ denotes the amplitude of the mains phase current (fundamental); U denotes the average value of the output voltage of the buck input stage, and $U_{N,l-l}$ denotes the rms value of the line-to-line voltage), one receives for the maximum output voltage of the buck input stage

$$U_{\max} = \frac{\sqrt{3}}{\sqrt{2}}\, U_{N,l-l}\, M_{\max}, \tag{4}$$

where at the case at hand the maximum modulation index is set to $M_{\max} = 0.9$ in order to have a margin to the theoretical limit $M'_{\max} = 1$ (cf. (3)) for system control.

If $U_{\max}$ is lower than the reference value U_0^* of the system output voltage U_0, the boost stage has to be activated, i.e., the on-time and/or duty cycle δ of the boost power transistor has to be set according to

$$\delta = 1 - \frac{U_{\max}}{U_0^*} \qquad \delta \in [0;1]. \tag{5}$$

Considering an input voltage range $U_{N,l-l} = (208 \ldots 480)\,\mathrm{V}$ and an output voltage $U_0 = 400\,\mathrm{V}$ the operating modes given in **Tab. 1** can be distinguished.

Operating Mode	$U_{N,l-l}$	M	δ
Buck+Boost	$(208 \ldots 360)\,\mathrm{V}$	0.9	$0.43 \ldots 0$
Buck	$(360 \ldots 480)\,\mathrm{V}$	$0.9 \ldots 0.68$	0

Table 1: Operating modes of the three-phase buck+boost PWM rectifier for wide input voltage range and a controlled output voltage of $U_0 = 400\,\mathrm{V}$.

In the following section, the different modulation methods (of the buck and of the boost stage) are given which do show different switching losses and different AC side behavior.

3 Modulation Methods

There are several possibilities for arranging the system switching states within one pulse half period. The resulting different switching state sequences (modulation methods) are depicted in **Fig. 4**. The active switching states can either be arranged symmetrically (cf. (1), (2) in **Tab. 2**) or asymmetrically (cf. (3) in Tab. 2) with reference to the middle of the pulse period, and the free-wheeling state can be placed in the middle (2) or at the beginning and/or at the end of a pulse half period, respectively (1). The different modulation methods are given in the following for a mains interval $\varphi_U \in (0; \frac{\pi}{6})$, for the sake of clearness, the free-wheeling state is shown in bold face.

If the switching power losses are assumed to be proportional to the switched current I and to the switched voltage, the modulation methods given in Tab. 2 show a ratio of the average values of switching power losses within one mains period of

$$P_{(1)} : P_{(2)} : P_{(3)} = 1 : \sqrt{3} : 2 \tag{6}$$

for given pulse frequency f_P. Accordingly, for equal switching losses pulse frequencies showing a ratio

$$f_{P,(1)} : f_{P,(2)} : f_{P,(3)} = 1 : 1/\sqrt{3} : 1/2 \tag{7}$$

Modulation method (1):

$$\Big|_{t_\mu=0} (101)\,(110)\,(\mathbf{000})\Big|_{t_\mu=T_P/2} (\mathbf{000})\,(110)\,(101)\Big|_{t_\mu=T_P}$$

Modulation method (2):

$$\Big|_{t_\mu=0} (101)\,(\mathbf{000})\,(110)\Big|_{t_\mu=T_P/2} (110)\,(\mathbf{000})\,(101)\Big|_{t_\mu=T_P}$$

Modulation method (3):

$$\Big|_{t_\mu=0} (101)\,(110)\,(\mathbf{000})\Big|_{t_\mu=T_P/2} (101)\,(110)\,(\mathbf{000})\Big|_{t_\mu=T_P}$$

Table 2: Different switching state sequences (modulation methods) for the buck input stage within one pulse period. t_μ denotes the local time being counted within the pulse period T_P, i.e., $t_\mu \in (0, T_P)$.

have to be selected [5].

For each switching state j with on-time δ_j, a line-to-line voltage is switched to the output of the buck stage. In **Tab. 3** the analytical expressions for the on-times δ_j and for the corresponding instantaneous values of the output voltage of the buck stage u_j are given for a mains phase voltage condition according to (1).

j	δ_j	u_j
(101)	$M\,(\frac{1}{2}\cos\varphi_U + \frac{\sqrt{3}}{2}\sin\varphi_U)$	$\hat{U}_{N,l-l}\cos(\varphi_U - \frac{\pi}{6})$
(110)	$M\,(\frac{1}{2}\cos\varphi_U - \frac{\sqrt{3}}{2}\sin\varphi_U)$	$\hat{U}_{N,l-l}\cos(\varphi_U + \frac{\pi}{6})$
(000)	$1 - M\,\cos\varphi_U$	0

Table 3: On-times δ_j and output voltages u_j for the switching states j within the mains interval $\varphi_U \in (0; \frac{\pi}{6})$.

The time behavior of the voltage u at the output of the buck stage within one pulse period is dependent on the selected modulation method (cf. Fig. 4), whereby the buck+boost inductor current ripple is influenced, but the modulation method does not take any influence on the average value of the voltage U appearing at the buck stage output,

$$U = (u_{(101)}\,\delta_{(101)} + u_{(110)}\,\delta_{(110)}) = \frac{\sqrt{3}\,U_{N,l-l}}{\sqrt{2}\,M}. \qquad (8)$$

In Fig. 6(a) the behavior of the buck output voltage u for an output power of $P_0 = 2.5\,\mathrm{kW}@U_{N,l-l} = 440\,\mathrm{V}$ and for an output voltage of $U_0 = 400\,\mathrm{V}$ is given for modulation method (1).

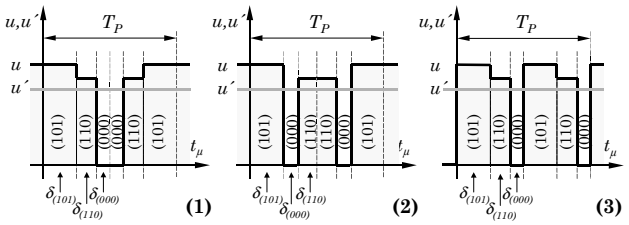

Fig. 4: Time behavior of the buck stage output voltage u within one pulse period for different modulation methods and deactivated boost stage ($\delta = 0$, i.e., $u' = \mathrm{const.} = U_0$).

If the boost stage has to be activated, i.e. if $\delta > 0$ is valid (cf. (5)), there are different possibilities of placing the switching function of the boost power transistor within the pulse (half) period, what does take influence on the voltage applied to the buck+boost inductor. The boost power transistor can either be activated during the free-wheeling state of the buck input stage (modulation method (1).1, cf. **Fig. 5**(a)) or during the active state of the buck stage (modulation method (1).2, cf. Fig. 5(b)). This effect is clearly shown in **Figs. 6**(b) and (c): Turning the boost power transistor on during the active switching states of the buck stage results in a significantly higher current ripple of the buck+boost inductor current as compared to Fig. 6(c), where the boost transistor is turned on while the buck input stage is operating in the free-wheeling state.

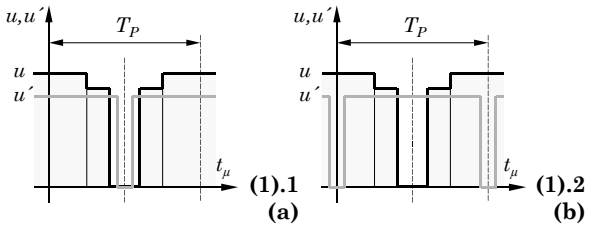

Fig. 5: Modulation of the boost stage. Voltage u at the output of the buck stage and voltage u' across the boost power transistor for placing the on-time of the boost converter power transistor in the buck stage free-wheeling interval (cf. **(a)**, modulation method (1).1); **(b):** operation of the boost converter power transistor shifted by $T_P/2$ in time as compared to (a) (modulation method (1).2).

Therefore, the time behavior of the ripple of the buck+boost inductor current is strongly dependent on the coordination of the modulation of the buck and of the boost stage. The ripple time behavior as well as the ripple rms value are calculated analytically in the following section.

4 Analytically Closed Calculation of the Buck+Boost Inductor Current Ripple

The current in the buck+boost inductor is determined by the voltage u at the output of the buck stage and by the voltage across the boost power transistor u' (which equals the system output voltage U_0 for disabled boost stage). One receives for the current ripple in the buck+boost inductor

$$\Delta i(t_{\mu,2}) = \frac{1}{L}\int_{t_{\mu,1}}^{t_{\mu,2}} \left[u(t_\mu) - u'(t_\mu)\right] \mathrm{d}t_\mu + \Delta i(t_{\mu,1}). \qquad (9)$$

The local rms value of the current ripple in dependency on the position φ_U of the pulse interval considered within the mains period can be calculated via

$$\Delta i^2_{rms}(\varphi_U) = \frac{1}{T_P/2}\int_{t_\mu=0}^{t_\mu=\frac{1}{2}T_P} \Delta i(t_\mu)^2 \mathrm{d}t_\mu = \qquad (10)$$

$$= \frac{2}{3\,T_P}\,[\; t_{\mu,1}\left(\Delta i_0^2 + \Delta i_0 \Delta i_{t_{\mu,1}} + \Delta i^2_{t_{\mu,1}}\right) +$$
$$(t_{\mu,2} - t_{\mu,1})\left(\Delta i^2_{t_{\mu,1}} + \Delta i_{t_{\mu,1}}\Delta i_{t_{\mu,2}} + \Delta i^2_{t_{\mu,2}}\right) +$$
$$(T_P/2 - t_{\mu,2})\left(\Delta i^2_{t_{\mu,2}} + \Delta i_{t_{\mu,2}}\Delta i_{T_P/2} + \Delta i^2_{T_P/2}\right)\Big]\,.$$

The global rms value of the DC current ripple within the mains period can be calculated by summation of the local rms values within one pulse half period,

$$\Delta I^2_{rms} = \frac{1}{T_N}\sum_k \Delta i^2_{rms}(\varphi_U). \qquad (11)$$

If the pulse frequency is substantially larger than the mains frequency (which is fulfilled in the case at hand) the summation can be replaced by an integration with good approximation,

$$\Delta I^2_{rms} = \frac{1}{\varphi_{U,2} - \varphi_{U,1}}\int_{\varphi_{U,1}}^{\varphi_{U,2}} \Delta i^2_{rms}(\varphi_U)\mathrm{d}\varphi_U. \qquad (12)$$

This allows an analytically closed calculation of the global rms value of the DC current ripple.

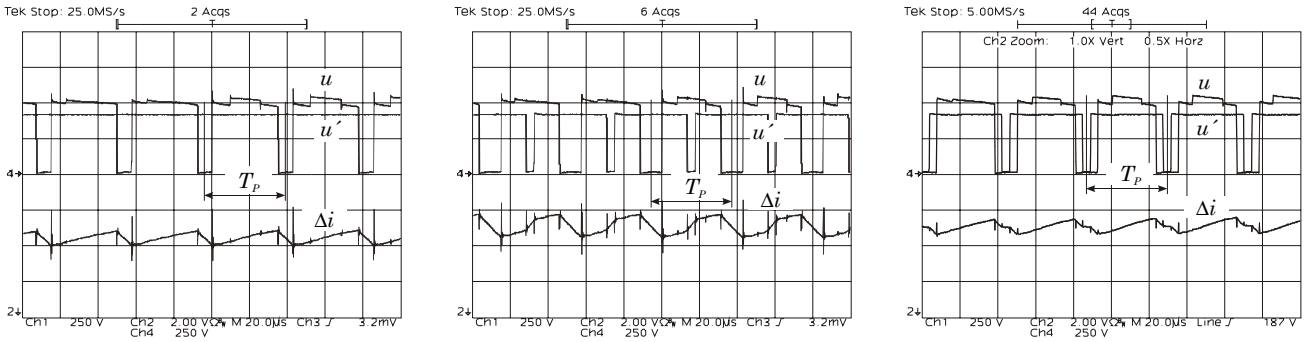

(a): Operation for disabled boost stage, $\delta = 0$.

(b): Boost operating during active state of buck stage.

(c): Boost operating during free-wheeling state of buck stage.

Fig. 6: Buck stage output voltage u, voltage u' across the boost power transistor and buck+boost inductor current ripple Δi for $P_0 = 2.5\,\mathrm{kW}$ @ $U_{N,l-l} = 440\,\mathrm{V}$. Voltage scale: 250 V/div; current scale: 2 A/div.

If we e.g. consider modulation method (1) for deactivated boost stage (cf. Fig. 4 (1)), one receives for the buck+boost inductor current ripple at the time instants $t_{\mu,i}$ within one pulse half period for a mains interval (1)

$$\begin{aligned} \Delta i_0 &= 0, \\ \Delta i_{t_{\mu,1}} &= 1/L\left(u_{(101)} - U_0\right)\delta_{101}T_P/2, \\ \Delta i_{t_{\mu,2}} &= 1/L\left(u_{(110)} - U_0\right)\delta_{110}T_P/2 + \Delta i(t_{\mu,1}), \\ \Delta i_{T_P/2} &= 0. \end{aligned} \tag{13}$$

The global rms value of the DC current ripple within one mains period can now be calculated incorporating the relative on-times δ_j and the output voltages u_j given in Tab. 3, (10) and (12) as well as the condition concerning the pulse frequencies (7); there the integration (12) can be limited to a $\frac{\pi}{6}$-wide mains interval and yields

$$\Delta I_{rms,(1)}/\Delta i_n = \tag{14}$$
$$= \frac{M}{8\sqrt{5\pi}}\sqrt{240\pi - M(600\sqrt{3}+352) + M^2(45\sqrt{3}+180\pi)},$$

with

$$\Delta i_n = \frac{\hat{U}_{N,l-l}}{2\sqrt{3}\,L\,f_P}\cdot\frac{1}{1-\delta}, \tag{15}$$

where $\delta = 0$ at the case at hand. For modulation methods (2) and (3) one receives for the global rms value of the DC current ripple

$$\Delta I_{rms,(2)}/\Delta i_n = \tag{16}$$
$$= \frac{\sqrt{3}M}{8\sqrt{5\pi}}\sqrt{180\pi - 90\sqrt{3} - 736M + M^2(180\pi - 135\sqrt{3})},$$

$$\Delta I_{rms,(3)}/\Delta i_n = \frac{M}{4\sqrt{10\pi}}\sqrt{120\pi - 704M + 105M^2\pi}. \tag{17}$$

In **Fig. 7** the results of the analytical calculations are compiled and compared with the simulation results, where an excellent conformity is given. Therefore, the very complex results of an analytical calculation of the global ripple current rms value for active boost output stage ($\delta > 0$) are omitted here for the sake of brevity. For the determination of the rms value of the buck+boost inductor current ripple for this case one could refer to the simulation results given in Fig. 10.

Incorporating (9) one can derive the local time behavior of the current ripple in the buck+boost inductor and its envelope for the different modulation methods. In **Fig. 8** the time behavior of the buck+boost inductor current ripple $\Delta i_{(i)}$ within a mains period is given for modulation methods (1) and (2) for disabled boost stage and a modulation index $M = 0.9$, **Fig. 9** shows the according envelopes $\Delta i_{\max,(i)}$ in dependency on the modulation index M of the buck input stage and on the mains angle φ_U for input voltage condition

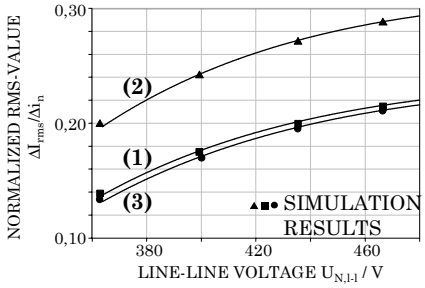

Fig. 7: Comparison of the results of a simulation (cf. Fig. 10) and of an analytical calculation of the rms value of the DC current ripple $\Delta I_{rms,(i)}$ for the different modulation methods (i) in case of deactivated boost output stage ($\delta = 0$).

according to (1). One can see immediately, that modulation method (2) having the free-wheeling state in the middle of one pulse half period does partly provide a lower DC current ripple. The comparison of Fig. 11 and Fig. 8 again shows the consistence between analytical calculation and simulation results.

The envelope of the DC current ripple of modulation method (3) does approximately equal modulation method (1) at $f_{P,(3)} = 2\,f_{P,(1)}$, a figure showing its dependency on the modulation index M and on the mains angle φ_U is

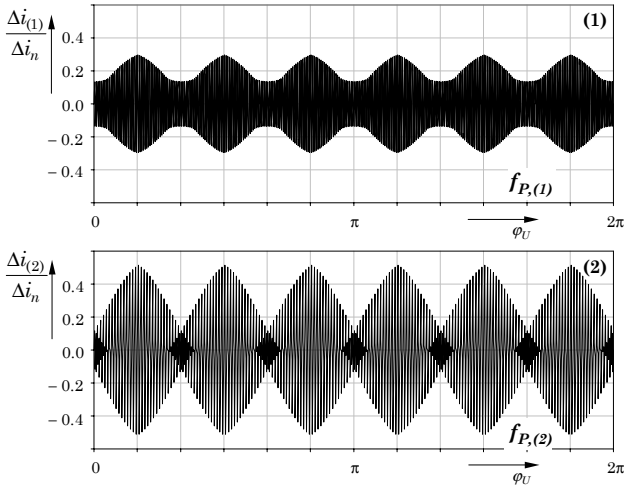

Fig. 8: Time behavior of the buck+boost inductor current ripple for modulation methods (1) and (2) within one mains period (modulation index $M = 0.9$). The pulse frequencies $f_{P,(1)}$ and $f_{P,(2)}$ are set according to (7). The boost stage is not active ($\delta = 0$).

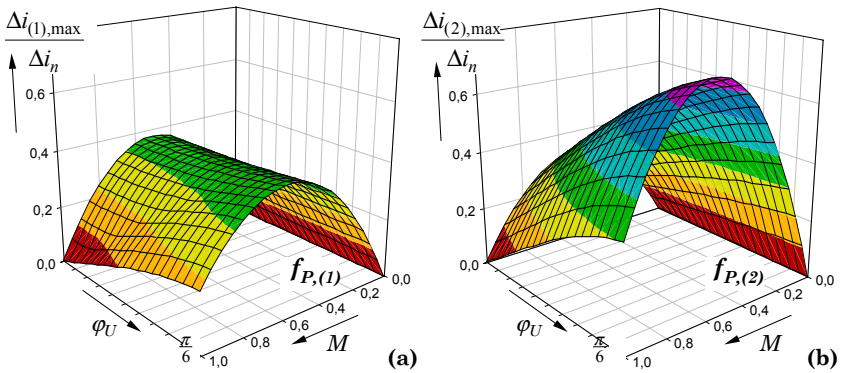

Fig. 9: Envelopes $\Delta i_{i,\max}$ of the normalized local buck+boost inductor current ripple Δi_i in dependency on the modulation index M for modulation methods (1) and (2) and for a mains phase voltage condition according to (1)). **(a):** modulation method (1), **(b):** modulation method (2); pulse frequencies $f_{P,(1)}$ and $f_{P,(2)}$ are set according to (7). The boost stage is not active ($\delta = 0$).

therefore omitted here for the sake of brevity.

The minimum load at which a transition between continuous conduction mode (CCM) and discontinuous conduction mode (DCM) occurs can be easily derived employing Fig. 9: in order to ensure CCM, the average value of the buck+boost inductor current I has to remain above the maximum amplitude of the current ripple $\Delta i_{(i)}$ occurring within one mains period. In case of boost converter operation ($\delta > 0$) the current ripple does decrease for modulation methods (1).1, (2) and (3) (cf. Fig. 11), hence DCM will not occur at the lower input voltage range for the same load condition.

5 Simulation Results

The time behavior of the buck+boost inductor current ripple for the different modulation methods has been analyzed by simulation using CASPOC® [6] with respect to (7) and the global rms value of the DC current ripple $\Delta I_{rms,(i)}$ was determined for the wide input voltage range $U_{N,l-l} = (208 \ldots 480)\,\mathrm{V}$ for an output voltage of $U_0 = 400\,\mathrm{V}$ by calculating the rms value online during the simulation. The results are normalized using (15) and are compiled in **Fig. 10**. **Figure 11** shows the simulation results of the time behavior of the buck+boost inductor current ripple Δi for the different modulation methods for

- disabled boost stage: $U_{N,l-l} = 380\,\mathrm{V}$, $U_0 = 400\,\mathrm{V}$, i.e., $M = 0.9$, and for
- boost converter operating: $U_{N,l-l} = 230\,\mathrm{V}$, $U_0 = 400\,\mathrm{V}$, i.e., $M = 0.9$ and $\delta = 0.4$.

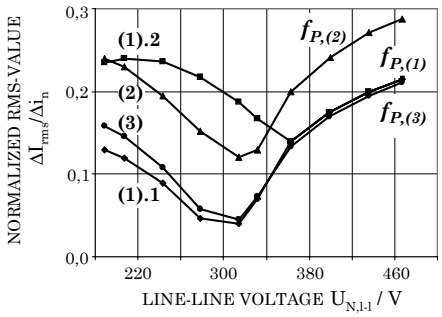

Fig. 10: Normalized rms value of the global buck+boost inductor current ripple $\Delta I_{rms,(i)}$ for the different modulation methods within a wide input voltage range.

The comparison of the global rms value of the different modulation methods shows that modulation method (1).1 is advantageous over all other modulation methods within the whole input voltage range in case of activated and/or deactivated boost output stage. Modulation methods (1) and (3) show the approximately the same rms value of the DC current ripple, but the pulse frequency of modulation method (1) is twice the pulse frequency of modulation method (3) for equal switching losses. As the comparison of modulation method (1).1 and (1).2 shows, the current ripple is clearly dependent on placing the switching function of the boost power transistor within the pulse (half) period: placing the active state of the boost power transistor during the active switching states of the buck input stage (cf. Fig. 5(b)) results in a rms value of the buck+boost inductor current ripple being ≈ 4.5 times higher in the worst case as compared to modulation method (1).1, where the boost stage power transistor turn-on interval is centered in the free-wheeling interval of the buck input stage (cf. Fig. 5(a)).

6 Experimental Results

In **Fig. 12** a comparison of the local and global time behavior of the buck+boost inductor current ripple Δi between simulation results and experimental results is given for $P_0 = 2.5\,\mathrm{kW}, U_{N,l-l} = 440\,\mathrm{V}, U_0 = 400\,\mathrm{V}$. There is a very good conformity of the simulated and experimental waveforms. Accordingly, the simulation results and/or the theoretical considerations can be considered to provide a sufficiently accurate description of the actual circuit behavior.

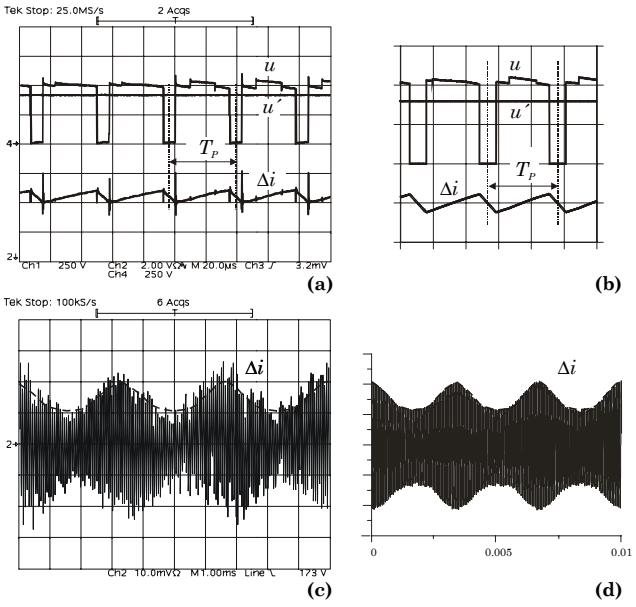

Fig. 12: Experimental results **(a),(c)** and related simulation results **(b),(c)** for disabled boost stage: Buck stage output voltage u, voltage across the boost power transistor $u' = U_0$ and DC current ripple Δi. Local time behavior (a),(b); global time behavior within one half mains period (c),(d). Scales: $u; u'$ in (a), (b): 250V/Div; Δi: 2A/Div.

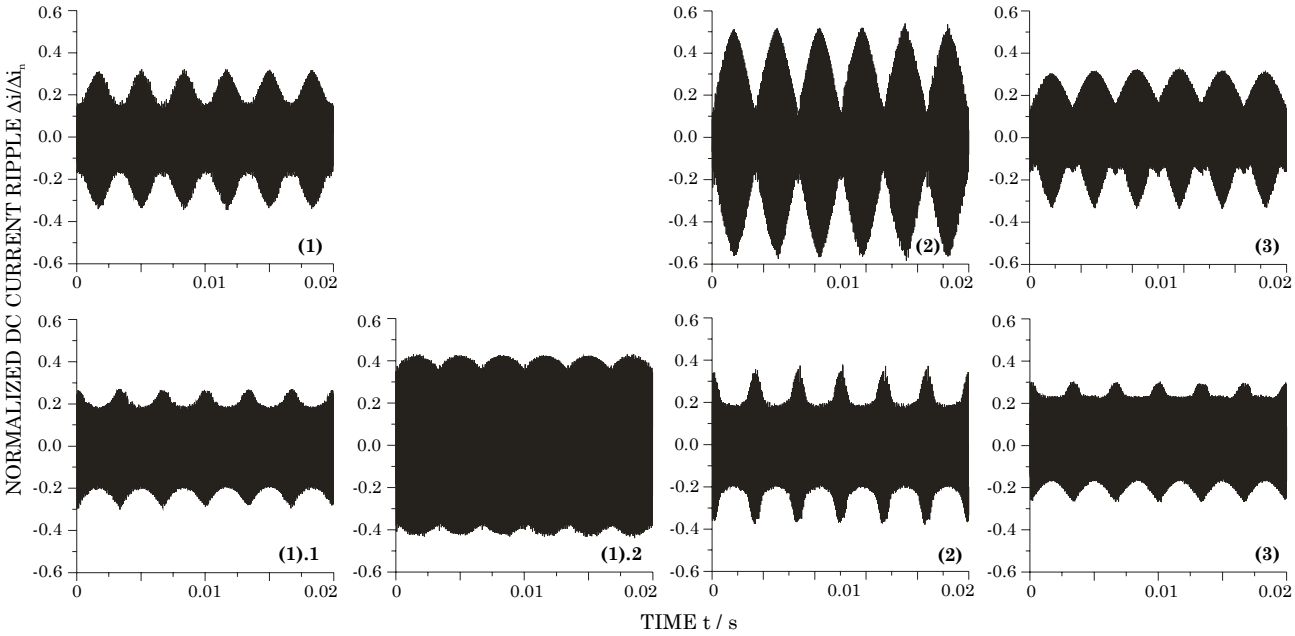

Fig. 11: Time behavior within one mains period of the normalized current ripple of the different modulation methods for disabled boost output stage ($\delta = 0$) and maximum modulation index $M = 0.9$ where $U_{N,l-l} = 380\,\mathrm{V}, U_0 = 400\,\mathrm{V}$ (top), and for boost stage operating at $\delta = 0.4$ and $M = 0.9$ where $U_{N,l-l} = 230\,\mathrm{V}, U_0 = 400\,\mathrm{V}$ (below). For modulation method (2) the turn-on interval of the boost stage power transistor is centered around the middle of each pulse period. For modulation method (3) the turn-on interval of the boost stage power transistor is placed just before the end of each pulse half period; the switching frequency is twice the buck stage pulse frequency and therefore is equal to modulation method (1) (cf. (7)).

7 Conclusions

In this paper, different modulation methods of a three-phase three-switch buck+boost unity power factor PWM rectifier are investigated concerning the time behavior and rms value of the buck+boost inductor current ripple. The modulation methods do differ concerning the arrangement of active and passive switching states of the buck input stage and the coordination of the switching of the buck input stage and the boost output stage within a pulse interval. The comparison shows that there exists one modulation method which does provide simultaneously a minimum DC current ripple and a minimum input filter capacitor voltage ripple at minimum switching losses and/or maximum pulse frequency. This optimum modulation method is characterized by the free-wheeling state of the buck input stage being placed at the beginning/at the end of one pulse half period, and by a turn-on interval of the boost stage power transistor being centered in the free-wheeling interval of the buck stage.

Due to the simultaneous minimization of input capacitor voltage ripple and output inductor current ripple and/or of AC and DC side behavior there is no way of further improving the DC side behavior by accepting lower AC side performance. Such trade-off would be possible in case the AC and DC side ripple minima would occur for different modulation schemes and would help to balance the largely different overall size of the AC side filter capacitors and the DC side filter inductor (cf. Fig.2). So, the only remaining possibility of minimizing the DC side inductor volume is a reduction of the inductance as far as possible. However this does result in a higher current ripple and in a higher sensitivity of the DC side current waveform concerning e.g., mains phase voltage unbalances and inaccuracies of the applied switching pattern due to, e.g. gate drive delay times or power semiconductor conduction voltage drops. (A control concept providing a proper pre-correction of the pulse pattern and/or turn-on times of the switches of buck and boost stage will be presented in a future paper.) Furthermore, the minimum load at which a transition from CCM to DCM occurs is shifted to higher values if the inductance is reduced. This could be compensated by activating the boost output stage. However, there one has to accept higher switching and/or higher conduction losses of the buck and of the boost stage.

A reduction of the size of the buck+boost inductor of given inductance could be achieved by magnetically biasing the inductor core by insertion of a permanent magnet. There eddy current losses in the permanent magnets are an issue to be considered. Furthermore, a local reduction of the buck+boost inductor current ripple and/or of the inductance for given ripple amplitude could be achieved by modulation of the buck stage carrier frequency with six times the mains frequency. Both approaches will be investigated in detail in the course of the continuation of the research.

References

[1] **Baumann, M., Drofenik, U., and Kolar, J. W.:** *New Wide Input Voltage Range Three-Phase Unity Power Factor Rectifier Formed by Integration of a Three-Switch Buck-Derived Front-End and a DC/DC Boost Converter Output Stage.* Proceedings of the 22^{nd} IEEE International Telecommunications Energy Conference, Phoenix, Arizona, U.S.A., Sept. 14 – 18, pp. 461–470 (2000).

[2] **Kolar, J. W.:** *Netzrückwirkungsarmes Dreiphasen-Stromzwischenkreis-Pulsgleichrichtersystem mit weitem Stellbereich der Ausgangsspannung.* Austrian Patent Application A9/2000, filed: Jan. 5, 2000.

[3] **Dahono, P.A., Sato, Y., and Kataoka, T.:** *An Analysis of the Ripple Components of the Input Current and Voltage of PWM Inverters.* Proceedings of the International Conference on Power Electronics and Drive Systems, Singapore, Feb. 21 – 24, Vol. 1, pp. 323 – 328 (1995).

[4] **Baumann, M., and Kolar, J. W.:** *Comparative Evaluation of Modulation Methods for a Three-Phase/Switch Buck Power Factor Corrector Concerning the Input Capacitor Voltage Ripple.* Proceedings of the 32^{nd} IEEE Power Electronics Specialists Conference, Vancouver, Canada, June 17 – 21, pp. 1327–1332 (2001).

[5] **Nishida, Y., and Maeda, A.:** *A Simplified Discontinuous-Switching-Modulation for Three-Phase Current-Fed PFC-Converters and Experimental Study for the Effects.* Proceedings of the 11^{th} IEEE Applied Power Electronics Conference, San Jose, California, U.S.A., March 3 – 7, pp. 552–558 (1996).

[6] **CASPOC -** *Power Electronics and Electrical Drives Modeling and Simulation.* www.caspoc.com.